Cardiac Electrophysiology using LS-DYNA®

Pierre L'Eplattenier[1], Inaki Caldichoury[1], Karim El Houari[2]

1 Ansys - Livermore Software Technology LLC
2 Ansys - Lyon Immeuble le Patio, 35-37 Rue Louis Guérin, 69100 Villeurbanne, France

1   Introduction

Heart disease is among the leading causes of death in the Western world; hence, a deeper understanding of cardiac functioning will provide important insights for engineers and clinicians in treating cardiac pathologies. However, the heart also offers a significant set of unique challenges due to its extraordinary complexity. In this respect, some recent efforts have been made to be able to model the multiphysics of the heart using LS-DYNA.

The model starts with electrophysiology (EP) which simulates the propagation of the cell transmembrane potential in the heart. This electrical potential triggers the onset of cardiac muscle contraction, which then results in the pumping of the blood to the various organs in the body. The EP/mechanical model can be coupled with a Fluid Structure Interaction (FSI) model to study the clinically relevant blood flow parameters as well as valves or cardiac devices. This paper concentrates on the EP part of the model.

Different propagation models, called "mono-domain" or "bi-domain", which couple the diffusion of the potential along the walls of the heart with ionic equations describing the exchanges between the inner and the outer parts of the cells have been implemented.
Other features of the EP solver will also be presented such as the coupling of the mono/bi domain models with a Purkinje Network, the automatic generation of fiber orientations, the computation of EKG, and the coupling of the EP with the mechanics and FSI.

2   Presentation of the model

The wall of the heart has three layers: epicardium, myocardium and endocardium. The endocardium and epicardium are thin layers consisting primarily of collagen and elastic tissue. In the middle layer, the myocardium, the cells that constitute the muscle show electrical excitability. These specialized cells, called myocytes, are organized into parallel cardiac fibers giving the muscle the striated appearance. The fibers form sheets which are connected by a collagenous network [1].
A cardiac cell (myocyte) is typically 10 to 20 µm in diameter and 80 to 125 µm in length. The cell membrane acts as an electrical insulator and contains ion channels which transport electrical current by diffusion. The potential difference across the membrane is called the transmembrane potential. Initially, a cardiac cell is at rest, with a potential difference across the membrane. The potential inside the cell is negative compared to the external, with a potential difference around 80mV. If the membrane potential rises to a certain threshold value (close to 40 mV) a rapid process occurs, during which different ions, mainly Na^+, K^+, and Ca^{2+}, are exchanged between the inner and the outer part of the cell, creating a fast depolarization, an early repolarization, a plateau and a final repolarization. The complete cycle of depolarization and repolarization lasts around 300 ms and is called "action potential". It is shown in Figure (1). This action potential diffuses from cell to cell through a network of gap junctions, creating a wave of depolarization and repolarization through the myocardium [1].
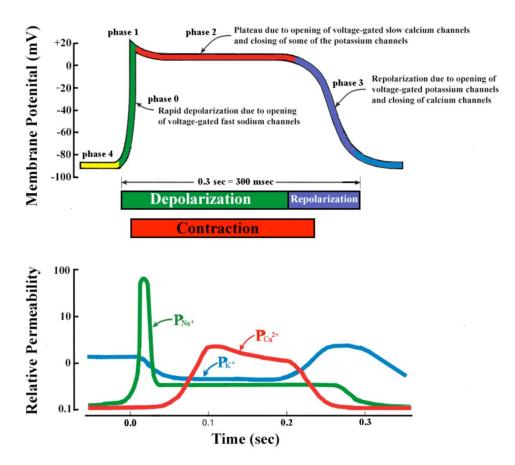
Fig.1: *A typical action potential of a ventricular myocyte and the underlying ion currents. The resting membrane potential is approximately ~80 mV (phase 4). The rapid depolarization is primarily due to the voltage gated Na+ current (phase 0), which results in a relatively sharp peak (phase 1) and transitions into the plateau (phase 2) until repolarization (phase 3). Also indicated are the refractory period and timing of the ventricular contraction. Modified from Tortora GJ, Grabowski SR. Principles of Anatomy and Physiology, ninth edition. New York: John Wiley & Sons, Inc., 2000*

2.1   The bidomain model

Since describing the whole heart, or even part of it like a ventricle, at the cell level would be computationally too expensive, continuous approximations are made, where the inner part of the cells is treated as one continuum "domain" with an inner potential $\phi_i(\vec{x}, t)$, and the outer part as another domain with an external potential $\phi_e(\vec{x}, t)$. Each domain is characterized by a conductivity tensor, called respectively σ_i and σ_e. These tensors are usually highly non-isotropic, with factors that can be as high as 5 to 10 between the conductivity along the fibers and the one across the fibers. Therefore, it is very important to correctly model the fiber orientation, which can be consumed from an imaging technique called the diffusion tensor MRI. A transmembrane current with surface density I_m flows between the two domains hence the so called "bi-domain" equations [2]:

$$\nabla \cdot (\sigma_i \nabla \phi_i) = \beta I_m \tag{1}$$
$$\nabla \cdot (\sigma_e \nabla \phi_e) = -\beta I_m \tag{2}$$

where β is the membrane surface to volume ratio.

This transmembrane current density I_m consists of a capacitive part, an ionic part generated by the cell membrane I_{ion}, and an imposed stimulation current density I_{stim}:

$$I_m = C_m \frac{\partial V_m}{\partial t} + I_{ion} + I_{stim} \tag{3}$$

where C_m is the membrane capacity per unit area, and we introduced the transmembrane potential:
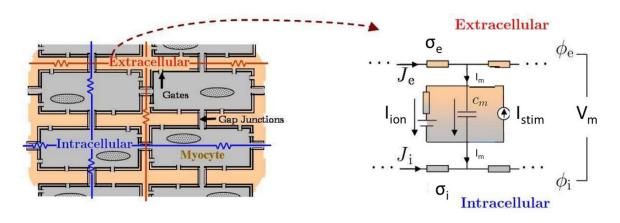
$$V_m = \phi_i - \phi_e \tag{4}$$

Fig.2: Illustration of the bidomain method (adapted from "Multiscale forward electromagnetic model of uterine contractions during pregnancy", La Rosa et al. BMC Medical Physics 2012, 12:4.).

Using (3) and (4), we can rewrite equations (1) and (2) in terms of V_m and ϕ_e as:

$$\beta C_m \frac{\partial V_m}{\partial t} + \beta I_{ion}(V_m, u) - \nabla \cdot (\sigma_i \nabla V_m) - \nabla \cdot (\sigma_i \nabla \phi_e) = \beta I_{stim}(\vec{x}, t) \tag{5}$$

$$\nabla \cdot (\sigma_i \nabla V_m) + \nabla \cdot ((\sigma_i + \sigma_e) \nabla \phi_e) = 0 \tag{6}$$

In equation (5), we wrote $I_{ion}(V_m, u)$, to indicate that the ionic current density depends not only on the transmembrane potential V_m, but also on an extra set of variables that we represent by u. The number of such variables and their time evolution depend on the cell model chosen, which we write, in a general way:

$$\frac{\partial u}{\partial t} = f(u, V_m) \tag{7}$$

These cell or „ionic" models locally describe the exchange of ions through the cell membrane, as schematically shown in Figure 1. More details about the Ionic models currently existing in LS-DYNA will be given in section (3).

Projecting equations (5) and (6) onto the FEM basis functions, we get:

$$\beta C_m M \frac{\partial V_m}{\partial t} + \beta I_{ion} - S_i V_m - S_i \phi_e = \beta I_{stim} \tag{8}$$

$$S_i V_m - S_{ie} \Phi_e = 0 \tag{9}$$

where

$$M(i,j) = \int_\Omega \varphi_i \varphi_j \, d\Omega \tag{10}$$

Is the mass matrix, and

$$S_i(i,j) = \int_\Omega \sigma_i \overrightarrow{\nabla \varphi_i} \, \overrightarrow{\nabla \varphi_j} \, d\Omega \tag{11}$$

and

$$S_{ie}(i,j) = \int_\Omega (\sigma_i + \sigma_e) \overrightarrow{\nabla \varphi_i} \, \overrightarrow{\nabla \varphi_j} \, d\Omega \tag{12}$$

are diffusion stiffness matrices corresponding to different conductivities.

In order to solve the coupled diffusion equations (8)-(9) with the ionic one (7), we use a so called "Spiteri-Ziaratgahi" operator splitting [3] where the advance from time t to time t+1 reads:

$$u(t+1) = u(t) + dt \, f(u(t), V_m(t), t) \tag{13}$$

$$\begin{bmatrix} \frac{\beta C_m}{dt} M + S_i & S_i \\ S_i & S_{ie} \end{bmatrix} \cdot \begin{bmatrix} V_m(t+1) \\ \phi_e(t+1) \end{bmatrix} = \begin{bmatrix} \frac{\beta C_m}{dt} M V_m(t) - \beta M I_{ion}(u(t+1), V_m(t), t) + \beta M I_{stim} \\ 0 \end{bmatrix} \tag{14}$$

2.2 The monodomain model

The monodomain model makes the extra hypothesis that the inner and outer conductivity tensors are proportional: $\sigma_e = \lambda \sigma_i$. We introduce a mean conductivity [2]:

$$\sigma = \frac{\sigma_i \sigma_e}{\sigma_i + \sigma_e} \tag{15}$$

or

$$\sigma_i = (1 + \lambda) \sigma \tag{16}$$

$$\sigma_e = \frac{1 + \lambda}{\lambda} \sigma \tag{17}$$

Equation (6) gives:

$$\nabla \cdot (\sigma_i \nabla \phi_e) = -\frac{\lambda}{1+\lambda} \nabla \cdot (\sigma_i \nabla V_m) \tag{18}$$

which gives, when using it in (5), an equation on V_m only:

$$\beta C_m \frac{\partial V_m}{\partial t} + \beta I_{ion}(V_m, u) - \nabla \cdot (\sigma \nabla V_m) = \beta I_{stim}(\vec{x}, t) \tag{19}$$

This is the monodomain equation.

When projecting equation (19) onto the FEM basis functions, we get:

$$\beta C_m M \frac{\partial V}{\partial t} + \beta I_{ion} - SV = \beta I_{stim} \tag{20}$$

with

$$S(i, j) = \int_\Omega \sigma \overrightarrow{\nabla \varphi_\imath} \; \overrightarrow{\nabla \varphi_\jmath} \; d\Omega \tag{21}$$

And M is defined by (10).

2.3   The extended monodomain model

The monodomain gives the transmembrane potential , but not the external potential nor the internal one. It is possible to rewrite equation (6) as [1]:

$$\nabla \cdot ((\sigma_i + \sigma_e) \nabla \phi_e) = -\nabla \cdot (\sigma_i \nabla V_m) \tag{22}$$

And solve this extra system to get the external potential, from which we can get the internal one using equation (4). It still is less expensive to solve the 2 smaller systems (19) and (22) than to solve the larger bidomain model (5)-(6) [4]. The user can decide about solving this extra system or not.

2.4   Benchmarks of the ls-dyna EP models

These models were first benchmarked against published results obtained from other EP research codes on a simple cuboid heart tissue model. More recently, we also performed benchmarks proposed by the FDA against analytical solutions. These benchmarks are presented in [5] and [6].

3   Cell Models

Depending upon the question of interest, one can select from a wide class of ionic models, ranging from the FitzHugh-Nagumo model [7][8] with two variables or the Fenton-Karma model with 3 variables [9] to the ten Tusscher and Panfilov model [10] with 19 variables and the Tomek [11] one with 43 variables.

The cell models are defined part-wise (except for the usermat one, which can depend on the nodes).

3.1   Fitzhugh-Nagumo

In the Fitzhugh-Nagumo model, the excitation is defined by a cubic polynomial along with one recovery variable, r [7],[8]. The transmembrane current, I_{ion}, is given by:

$$I_{\text{ion}} = -C_m \frac{\partial V}{\partial t} = -cV (V - \alpha)(V - 1) - rV \tag{23}$$

Here V is the transmembrane potential, C_m is the specific capacitance of the cell membrane, and c and α are excitation constants.

The recovery variable r evolves according to:

$$\frac{dr}{dt} = (\gamma + \frac{r\mu_1}{\mu_2 + V})(-r - cV(V - \beta - 1)) \tag{24}$$

where β, γ, μ_1 and μ_2 are excitation constants.

3.2   Fenton-Karma

The Fenton-Karma model is a simplified ionic model with three membrane currents that approximates well the restitution properties and spiral wave behavior of more complex ionic models of cardiac action potential (Beeler-Reuter and others). It was introduced in [9].

The total current flowing through the membrane is given by:

$$I_{\text{ion}} = -C_m \frac{\partial V}{\partial t} = -J_{\text{fi}} \tag{25}$$

where V is the transmembrane potential, C_m is the specific capacitance of the cell membrane, and J_{fi} is the fast inward current.

The model depends on three state variables, u, v, and w, and three membrane currents, J_{fi}, J_{so} (slow outward current), and J_{si} (slow inward current), through the following equations:

$$\frac{du}{dt} = -J_{\text{fi}} - J_{\text{so}} - J_{\text{si}} \tag{26}$$

$$\frac{dv}{dt} = \frac{\Theta(u_c - u)(1 - v)}{\tau_{vm}} - \frac{\Theta(u - u_c)v}{\tau_{vp}} \tag{27}$$

$$\frac{dw}{dt} = \frac{\Theta(u_c - u)(1 - w)}{\tau_{wm}} - \frac{\Theta(u - u_c)w}{\tau_{wp}} \tag{28}$$

$$J_{\text{fi}} = -\frac{\Theta(u_c - u)(1 - u)(u - u_c)}{\tau_d} \tag{29}$$

$$J_{\text{so}} = \frac{u\,\Theta(u_c - u)}{\tau_o} + \frac{u\,\Theta(u - u_c)}{\tau_r} \tag{30}$$

$$J_{\text{si}} = -\frac{w(1 + \tanh[k(u - u_c^{si}])}{2\tau_{si}} \tag{31}$$

In the above Θ is the Heaviside step function.

3.3   Ten-Tusscher

This is a model of the action potential of human ventricular cells that, while including a high level of electrophysiological detail, is computationally cost-effective enough to be applied in large-scale spatial simulations for the study of reentrant arrhythmias. This model is based on [10].

3.4   Tomek

The Tomek model [11] is a human-based ventricular model for simulations of electrophysiology and excitation-contraction coupling, from ionic to whole-organ dynamics, including the electrocardiogram. It can be used under healthy conditions, but also with key disease conditions, and can include the effect of different drugs.

3.5   User defined cell models using define functions

A user can define his own cell model either through define functions or using usermat. When using define functions, different define functions are used to define the evolution of the state variables as a function of time, time step and the values of the other state variables. The model is composed of the transmembrane potential, V, along with n state variables $u_1, u_2, \dots u_n$. Their temporal evolution is given either as:

$$V(t) = g\big(t, dt, V(t-1), u_1(t-1), u_2(t-1), \dots, u_n(t-1)\big)$$
$$u_1(t) = f_1\big(t, dt, V(t-1), u_1(t-1), u_2(t-1), \dots, u_n(t-1)\big)$$
$$u_2(t) = f_2\big(t, dt, V(t-1), u_1(t-1), u_2(t-1), \dots, u_n(t-1)\big)$$
$$\vdots$$
$$u_n(t) = f_n\big(t, dt, V(t-1), u_1(t-1), u_2(t-1), \dots, u_n(t-1)\big)$$

Or as

$$\frac{\partial V(t)}{\partial t} = g\big(t, dt, V(t-1), u_1(t-1), u_2(t-1), \dots, u_n(t-1)\big)$$
$$\frac{\partial u_1(t)}{\partial t} = f_1\big(t, dt, V(t-1), u_1(t-1), u_2(t-1), \dots, u_n(t-1)\big)$$
$$\frac{\partial u_2(t)}{\partial t} = f_2\big(t, dt, V(t-1), u_1(t-1), u_2(t-1), \dots, u_n(t-1)\big)$$
$$\vdots$$
$$\frac{\partial u_n(t)}{\partial t} = f_n\big(t, dt, V(t-1), u_1(t-1), u_2(t-1), \dots, u_n(t-1)\big)$$

Where define functions are used to define $g, f_1,\ f_n$, and other ones are used to define the initial values of $V, u_1,\ u_n$ as a function of (x,y,z) and other parameters.

3.6 User defined cell models using usermat

The user can also define a cell with a usermat subroutine in dyn21em.f. In this subroutine, the user initialises the state variables and the constants of the model at the initial time step, and defines the advance of these variables by one time step at subsequent time steps.
This allows to have more complex cell models than the define functions. It also offers the flexibility to have different cell models (with different number of state variables) at each node, or in different areas of the ventricles, atria, ...

4 Purkinje Network

The Purkinje network is a specialized conduction system within the heart that ensures the proper activation of the ventricles to produce effective contraction. During the ventricular contraction portion of the cardiac cycle, the Purkinje fibers carry the contraction impulse from both the left and right bundle branch to the myocardium of the ventricles. This causes the muscle tissue of the ventricles to contract and generate force to eject blood out of the heart, either to the pulmonary circulation from the right ventricle or to the systemic circulation from the left ventricle. The Purkinje network is thus an important part of the excitation system in the human heart, which is shown in figure 3. Yet, up to now, there is no in vivo imaging technique to accurately reconstruct its geometry and structure. Computational modeling of the Purkinje network is increasingly recognized as an alternative strategy to visualize, simulate, and understand the role of the Purkinje system.
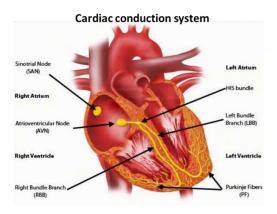

Fig.3: Cardiac conduction system showing the Purkinje fibers.

We thus developed an automatic 3D fractal network generation on a non-smooth surface (here, the endocardial surface of the ventricle), which is coupled to the 3D volume mesh, in a similar way as described in [12]. This Purkinje network is composed of conducting beams, and the leaves of the network are connected to the nodes of the volume mesh of the ventricle, thus allowing a coupling of the EP waves between the Purkinje network and the ventricles. Figure 4 shows such a network on a simple by-chamber surface, as well as the EP wave propagation on a Purkinje network coupled with a ventricle.
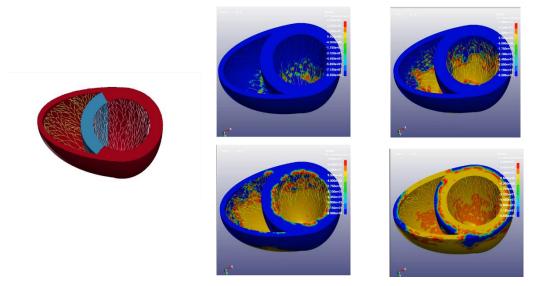

Fig.4:   Example of 2 purkinje networks in a bi-chamber simulation (left) and propagation of the transmembrane potential (right) showing the fast propagation through the network and the slower diffusion through the tissue.

5   Fiber Orientation

An automatic generation of fiber orientations, which can be used in EP with orthotropic conductivity tensors σ_i and σ_e, as well as in the mechanical model *MAT_295, can be done using the card *EM_EP_CREATEFIBERORIENTATION. It is based on [13]; where the user gives node or segment set to define the dirichlet constraints of the different Laplace system to solve in order to get the potentials and their gradients, as well as some define functions to set up α and β in each element, so that a local coordinate system can be defined. This is explained schematically in figure (5), and the corresponding result is shown on figure (6).
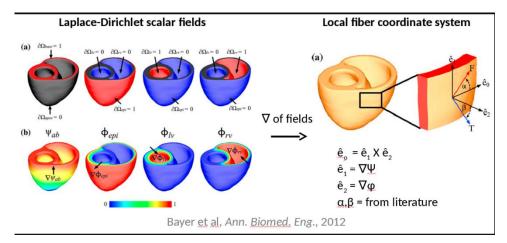

*Fig.5:   Illustration (from [13]) of the construction of fiber orientations using the card *EM_EP_CREATEFIBERORIENTATION.*
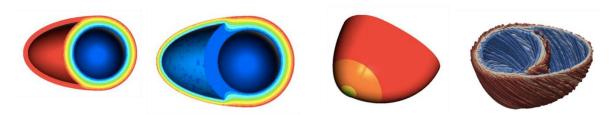
Fig.6:   Fiber orientations on a bi-chamber example using *EM_EP_CREATEFIBERORIENTATION

6   Computation of EKG

From the transmembrane potential V_m in the tissue, one can compute the external potential ϕ_e at different locations on the torso, even if the torso is not included in FEM the domain, using the integral [14]:

$$\Phi_e(x_e) = -\int_b \nabla\Phi \cdot \nabla \frac{1}{||x - x_e||} dV$$

The card *EM_EP_EKG allows to define a set of points x_e where the external potential Φ_e is computed at different time steps. Different combinations of these external potentials then allows to compute the EKG signals.
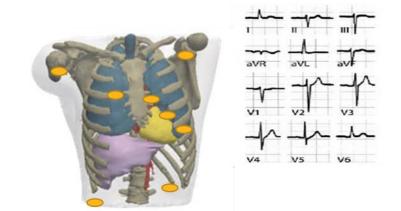

Fig.7:   Example of an EKG computations

7   Coupling with mechanics and FSI

The EP models give the local and temporal transmembrane potential as well as intracellular calcium ion concentration which provide the activation part of the heart muscle myofilament models, hence the input for the mechanical tissue models. An anisotropic hyperelastic constitutive model, including an active term, *MAT_295, was developed in order to couple the EP with the mechanical deformations. These deformations can furthermore be coupled with the hemodynamics using the fluid-structure interaction (FSI) capabilities of the ICFD module of LS-DYNA. Figure 8 shows an example of a coupled EP-mechanics-FSI simulation.
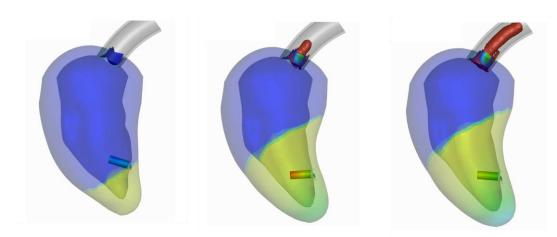
Fig.8:   Ventricular contraction showing the propagation of the EP wave, the contraction of the ventricle, and the blood flow through the valve

8   Summary

An EP solver was introduced in LS-DYNA. Both monodomain and bidomain methods have been developed, with different algorithms for each of them. An extended-monodomain model where the internal and external potentials can also be computed is available. The 3 models can be coupled together in the same simulation and a surrounding bath can also be added.
The mono and bidomain model models can be coupled to different cell models, including FitzHugh-Nagumo, Fenton-Karma, ten Tusscher and Panfilov, Tomek and user-defined ones. The mono and bi-domain models can also be coupled with a Purkinje network which can be automatically generated on the endocardial surface of the ventricle. Fiber orientations, which are used by both the EP and mechanical models can also be automatically built.

Our goal is to be able to simulate a full heart beat, so the EP solver can be coupled with an anisotropic hyperelastic constitutive model so that the EP wave can generate the deformation of the ventricles or atria which in turn can be coupled with the ICFD module to solve the hemodynamics part of the problem.

9   Literature

[1] Ruth Aris Sanchez, Electromechanical Large Scale Computational Models of the Ventricular Myocardium, PhD Thesis, Universitat Politecnica de Catalunya, Sept. 2014.
[2] Mark Potse, Bruno Dubé, Jacques Richer, Alain Vinet, and Ramesh M. Gulrajani, A Comparison of Monodomain and Bidomain Reaction-Diffusion Models for Action Potential Propagation in the Human Heart, IEEE Trans. Biomed. Eng., vol. 53, no. 12, 2006.
[3] M.E. Marsh, S.T. Ziaratgahi, and R.J. Spiteri, The secrets to the success of the Rush-Larsen method and its generalizations, IEEE Trans. Biomed. Engrg., 59(9):2506-2515., 2015
[4] M. Potse, B. Dube, J. Richer, A. Vinet and R. M. Gulrajani, "A Comparison of Monodomain and Bidomain Reaction-Diffusion Models for Action Potential Propagation in the Human Heart," in IEEE Transactions on Biomedical Engineering, vol. 53, no. 12, pp. 2425-2435, Dec. 2006, doi: 10.1109/TBME.2006.880875.
[5] P.L'Eplattenier et Al, „Cardiac Electrophysiology Using LS-DYNA" proceedings of the 15th Internaltional LS-DYNA Users Conference, Dearborn, May 2018
[6] P.L'Eplattenier et Al, „Cardiac Electrophysiology Using LS-DYNA" proceedings of the 16th Internaltional LS-DYNA Users Conference, Dearborn, May 2020
[7] FitzHugh R. Mathematical models of threshold phenomena in the nerve membrane. Bull. Math. Biophysics, 17:257—278, 1955
[8] Nagumo J., Arimoto S., and Yoshizawa S. An active pulse transmission line simulating nerve axon. Proc IRE. 50:2061–2070, 1962
[9] Fenton FH, Karma A., Vortex dynamics in three-dimensional continuous myocardium. Filament instability and fibrillation. Chaos 8: 20-47, 1998

[10] K. H., W. J., ten Tusscher, A.V. Panfilov, Alternans and spiral breakup in a human ventricular tissue model, Am. J. Physiol. Heart Circ., Physiol 291: H1088-H1100, 2006.

[11] Development, calibration, and validation of a novel human ventricular myocyte model in health, disease, and drug block, J. Tomek et al, eLife 2019;8:e48890 DOI: 10.7554/eLife.48890

[12] F.S. Costabal & Al, J Biomech, "Generating Purkinje Networks in the Human Heart" 2016 August 16; 49(12): 2455–2465.

[13] Bayer, J.D., Blake, R.C., Plank, G. et al. A Novel Rule-Based Algorithm for Assigning Myocardial Fiber Orientation to Computational Heart Models. Ann Biomed Eng 40, 2243–2254 (2012). https://doi.org/10.1007/s10439-012-0593-5

[14] Gima, K., and Rudy, Y. (2002). Ionic current basis of electrocardiographic waveforms: a model study. *Circ. Res.* 90, 889–896. doi: 10.1161/01.res.0000016960.61087.86